International Journal of Structural Stability and Dynamics
(2023) 2350160 (29 pages)

DOI: 10.1142/S0219455423501602

Analytical Model for Thermoelastic Dissipation in Oscillations of Toroidal Micro/Nanorings in the Context of Guyer–Krumhansl Heat Equation

Abduladheem Turki Jalil*, Sabah Auda AbdulAmeer†, Yaser Mohammed Hassan‡, Ibrahim Mourad Mohammed§, Malak Jaafar Ali¶, Zahraa Hassan Ward||, Saeid Ghasemi**,††,‡‡

*Medical Laboratories Techniques Department
Al-Mustaqbal University College, Babylon Hilla, 51001, Iraq

†Ahl Al Bayt University, Kerbala, Iraq

‡Engineering Technical College
Al-Farahidi University, Baghdad, Iraq

§Al-Nisour University College, Baghdad, Iraq

¶Department of Medical Laboratory Technics
AlNoor University College, Nineveh, Iraq

||Mazaya University College, Iraq

**Department of Mechanical Engineering
Amirkabir University of Technology, Tehran, Iran
††saeid.ghasemi12964@gmail.com

Received 1 November 2022
Revised 8 January 2023
Accepted 16 January 2023
Published 6 March 2023

Thermoelastic dissipation or thermoelastic damping (TED) can restrict the quality factor of micro/nanoring resonators seriously. This paper employs the non-Fourier model of Guyer–Krumhansl (GK model) to render a size-dependent formulation and analytical solution for approximating the amount of TED in micro/nanorings with circular cross-section by inclusion of nonlocal and single-phase-lagging effects. To fulfill this objective, the equation of heat conduction in the ring is first established according to GK model. Then, by placing the temperature distribution obtained from the heat conduction equation in the TED relation defined on the basis of thermal energy approach, an expression in the form of infinite series is given for TED, which includes non-classical parameters of GK model. Finally, after checking the validity of the model through a comparative study, several simulation results are prepared to emphasize on the influence of different factors such as non-classical parameters of GK model, geometry of ring, vibrational mode and ambient temperature on TED value. Numerical examples reveal that the mentioned

‡‡Corresponding author.

factors along with the two- or three-dimensional heat transfer (2D or 3D) model have major influences on TED variations.

Keywords: Thermoelastic damping; micro/nanoring resonators; circular cross-section; Guyer–Krumhansl model; non-Fourier effect.

Nomenclature

Symbol (unit)	Description of the symbols
$R\,(\mathrm{m}),\ \theta\,(\mathrm{rad})$ and $Z(\mathrm{m})$	: Principal directions of global cylindrical coordinate system
$x\,(m), y\,(m)$ and $z\,(m)$	: Principal directions of local Cartesian coordinate system
$r\,(\mathrm{m})$ and $\phi\,(\mathrm{rad})$	: Principal directions of local polar coordinate system
$R_0\,(\mathrm{m})$ and $r_0\,(\mathrm{m})$	: Mean and cross-sectional radius of ring, respectively
$w\,(\mathrm{m})$	: Radial displacement
$\sigma_{\theta\theta}\,(\mathrm{Pa})$	: Tangential normal stress
ε_{RR}, $\varepsilon_{\theta\theta}$ and ε_{zz}	: Radial, tangential and axial normal strains, respectively
ε_{ii}	: Trace of strain tensor
$E\,(\mathrm{Pa}),\ \nu$ and $\rho\,(\mathrm{kg/m^3})$	: Elasticity modulus, the Poisson ratio and mass density, respectively
$\alpha\,(1/K),\ k\,(\mathrm{W/mK})$ and $c_v\,(\mathrm{J/kgK})$	: Thermal expansion coefficient, thermal conductivity and specific heat per unit mass, respectively
$T_i\,(\mathrm{K}),\ T_a\,(\mathrm{K})$ and $T(\mathrm{K})$	: Instantaneous temperature, ambient temperature and temperature change, respectively
$t\,(\mathrm{s})$	: Time
$\boldsymbol{q}(\mathrm{W/m^2})$	: Heat flux vector
$\tau\,(s)$ and $l\,(\mathrm{m})$	: Relaxation time and nonlocal parameter, respectively
$\chi\,(\mathrm{m^2/s})$ and Δ_E	: Thermal diffusivity and relaxation strength, respectively
n	: Mode number of vibration
$\omega_n\,(\mathrm{rad/s})$	: The nth frequency of vibration
$I\,(\mathrm{m^4})$ and $A\,(\mathrm{m^2})$	: Moment of inertia of cross-sections and cross-sectional area, respectively
$\hat{\sigma}_{\theta\theta}\,(\mathrm{Pa})$ and $\hat{\varepsilon}_{\theta\theta}$	: Maximum value of tangential normal stress and strain, respectively

$\Delta U\,(J)$ and $U_{\max}\,(J)$: Dissipated thermal energy and maximum strain energy per cycle, respectively
Q_{3D}^{-1} : Inverse of three-dimensional quality factor

1. Introduction

Since micro/nano electromechanical systems (MEMS/NEMS) possess distinctive attributes such as low volume, small dimensions, use of little energy and high persistence, the demand for their use in scientific and engineering communities has increased day by day. Micro/nanoring resonators are favorite components utilized in MEMS/NEMS. Owing to their simple shape, small-sized rings are extensively exploited as components of vibratory gyroscopes,[1] rate sensors,[2] multi-axis angular velocity sensors,[3] dual-mode MEMS-based resonators,[4] force sensor,[5] the electro-optical modulator,[6] ultrasonic-motor actuator,[7] label-free sensor,[8] etc. According to the increasing demand for the use of this category of resonators, the issue of energy loss and achieving a high-quality factor is one of the key goals in their optimal design. The most well-known and widely used of these rings are those with rectangular or circular cross-section.

In the classical Fourier model of heat conduction, it is assumed that the transmission of thermal signals in solid bodies is carried out at an infinite speed. This assumption clearly contradicts the heat transfer in some special cases. According to several experimental tests, the validity of the Fourier model is challenged in conditions like large temperature gradients, thermal shocks, high-rate heating, short-time response and small scales.[9,10] Hence, several non-Fourier heat conduction models or generalized thermoelasticity theories have been introduced to improve the classical model. Lord and Shulman[11] incorporated a relaxation time parameter within the Fourier model to develop their model (LS model) and capture size effect in time domain. For taking into account the size effect in both time and space domains, Tzou[12] proposed the dual-phase-lag (DPL) model by accommodating two-phase lag parameters into the classical Fourier model. By inclusion of both phase-lagging and nonlocal effects in the Fourier model, Guyer and Krumhansl[13] established a mathematical description (GK model) for heat conduction in solid media. Green and Naghdi[14] put forward a model called GN-III model in which the propagation of thermal signals is characterized in an area with energy loss and high-rate excitation.

Theoretical and empirical researches have revealed that thermoelastic damping (TED) is a significant energy dissipation mechanism in micro/nanoresonators at room temperature. TED is caused by irreversible thermal currents in an oscillating thermoelastic solid. Thereby, it is impossible to be absolutely omitted by improving the manufacturing process. Accordingly, precious estimation of TED value for

optimizing the design of high-quality factor miniaturized structures is decisive. By means of the Fourier model, the first mathematical model for calculating TED in Euler–Bernoulli beams was provided by Zener[15] on the basis of thermal energy approach. Years later, Lifshitz and Roukes[16] arrived at a simple and single-term expression for TED in Euler–Bernoulli beams within the framework of the frequency approach. After that, by exploiting different models of heat conduction, many articles about TED in micro/nanostructures have been published.

Wong *et al.*[17] employed frequency approach to derive a closed-form solution for computing TED value in rectangular cross-sectional rings. Lu *et al.*[18] applied the Donnell–Mushtari–Vlasov (DMV) equations for thin shells in the context of classical continuum theory (CT) and the Fourier model to evaluate TED in miniaturized cylindrical shells. By utilizing the Fourier model, Li *et al.*[19] developed a mathematical model to determine TED value in circular and rectangular microplates with the aid of thermal energy approach. In the work of Fang and Li,[20] thermal energy approach as well as the 2D Fourier model have been used to attain an analytical solution for calculation of TED value in thin rings with rectangular cross-section. In studies similar to the paper published by Fang and Li,[20] Zhou *et al.*[21] and Zhou and Li[22] examined the influence of phase lag parameters on TED value in rectangular cross-sectional micro/nanorings via LS and DPL models, respectively. For clarifying small-scale effect on the magnitude of TED in circular nanoplates, in the context of nonlocal theory (NT) and DPL model, Xiao *et al.*[23] provided an exact solution for TED. Within the framework of both 2D and 3D models for heat conduction, TED in miniaturized rings with circular cross-section has been appraised based on the Fourier and LS models by Li *et al.*[24] and Kim and Kim,[25] respectively. In the paper of Li and Esmaeili,[26] NT together with GK model has been used to attain a model computing TED value in axisymmetric circular nanoplates. Tai and Chen[27] employed CT and the Fourier model to establish an analytical model for evaluation of TED in out-of-plane vibrations of rectangular cross-sectional microrings. By means of fractional order theory of thermoelasticity, Abbas and Hobiny[28] investigated the impact of non-classical parameters on TED in small-sized beam resonators. By simultaneously applying the modified couple stress theory (MCST) and nonlocal dual-phase-lag (NDPL) model, Zhou *et al.*[29] developed a size-dependent model for TED in small-scaled rings with circular cross-section. According to MCST and three-phase-lag (TPL) heat conduction model, Kumar and Mukhopadhyay[30] derived an explicit solution for TED in the Kirchhoff rectangular microplates. Zhou *et al.*[31] established analytical TED models for fully clamped and simply supported rectangular plates by accounting for 3D case of GK heat conduction model. In the research of Zhou and Li,[32] TED in miniaturized rectangular and circular plates has been surveyed by way of MCST and nonlocal version of DPL model. By exploiting MCST and DPL model, Borjalilou and Asghari[33] proposed an analytical model for estimating TED value in electrically actuated microresonators. In the context

of GK model, Zhou *et al.*[34] proposed 1D and 2D models for TED in rectangular cross-sectional micro/nanoring resonators. In addition to the mentioned studies, many other investigations have been accomplished on the analysis of mechanical and thermoelastic behaviors of beams,[35–61] plates,[62–75] shells[76–82] and thermoelastic media.[83–91]

As per the topics discussed above, among the various mechanisms of energy loss in mechanical components with micron and submicron dimensions, TED is of particular significance in a way that can disrupt their optimal performance. The literature review also reveals that heat conduction in such small structures is absolutely influenced by size. Given these two issues, one can deduce that employing non-Fourier models of heat transfer plays a vital role in computing the correct value of TED in micro/nanostructures. To the best of authors' knowledge, this is the first study that renders a mathematical simulation and analytical solution for TED in rings with circular cross-section in the purview of non-Fourier model of Guyer–Krumhansl. Given that this model reflects both phase-lagging and nonlocal effects, it is more comprehensive than Fourier and LS models, and leads to more accurate predictions. To establish a model on the basis of GK model, in the first step, the equation of heat conduction in the circular cross-sectional ring is extracted within the framework of this non-classical model. By substituting the profile of temperature derived from the equation of heat conduction in the TED relation introduced via thermal energy approach, an analytical formula containing phase lag and nonlocal parameters is then established for TED. In the end, after assessment of the correctness of the presented formulation by performing a comparison study, various numerical examples are provided to enlighten the role of some significant factors like non-classical parameters of GK model, dimensions of ring, vibration mode number and reference temperature in the variations of TED.

2. Problem Definition

Consider a circular cross-sectional ring with mean radius R_0 and cross-sectional radius r_0, as shown in Fig. 1. A global cylindrical coordinate system (R, θ, Z) is fixed at the center of ring. Moreover, a local coordinate system (x, y, z) is attached to the cross-section of the ring. Furthermore, parameter ϕ refers to the local angle. The radial displacement is also represented by w. Hence, the tangential strain is given by:[24]

$$\varepsilon_{\theta\theta} = -\frac{x}{R_0^2}\left(w + \frac{\partial^2 w}{\partial \theta^2}\right). \tag{1}$$

According to thermoelastic constitutive relation, one can write[24]

$$\varepsilon_{\theta\theta} = \frac{\sigma_{\theta\theta}}{E} + \alpha T, \tag{2}$$

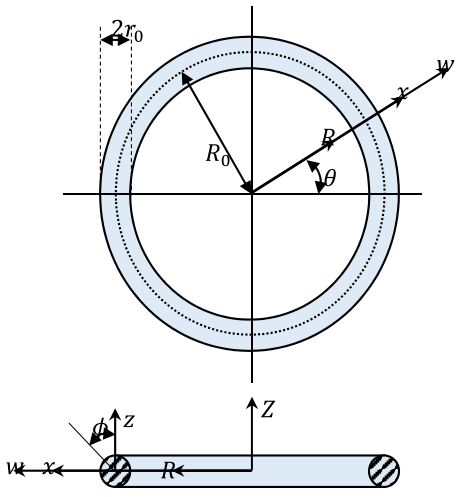

Fig. 1. Configuration of a circular cross-sectional ring.

where $\sigma_{\theta\theta}$ is the tangential normal stress. Material constants E and α stand for the elasticity modulus and coefficient of thermal expansion, respectively. In addition, variable $T = T_i - T_a$ represents the temperature change with T_i and T_a as instantaneous and ambient temperatures, respectively. According to Eq. (2), one can obtain:

$$\sigma_{\theta\theta} = E\varepsilon_{\theta\theta} - E\alpha T. \tag{3}$$

Constitutive relations in two other directions have the following form:[24]

$$\varepsilon_{RR} = \varepsilon_{zz} = -\nu\frac{\sigma_{\theta\theta}}{E} + \alpha T, \tag{4}$$

where parameter ν denotes the Poisson ratio. Moreover, ε_{RR} and ε_{zz} stand for the normal strains in the direction of R and z, respectively.

Within the framework of the Guyer–Krumhansl (GK) model, the constitutive relation of heat conduction is written as follows:[10]

$$\boldsymbol{q} + \tau\frac{\partial \boldsymbol{q}}{\partial t} = -k\boldsymbol{\nabla}T + l^2[\nabla^2\boldsymbol{q} + 2\boldsymbol{\nabla}(\boldsymbol{\nabla}q)], \tag{5}$$

in which $\boldsymbol{q}$ denotes the vector of heat flux. Symbol $\boldsymbol{\nabla}$ refers to the gradient vector. Moreover, parameter k is the thermal conductivity of medium. Material constant τ is also known as relaxation time or heat flux phase lag parameter. Furthermore, parameter l refers to nonlocal parameter.

The equation of conservation of energy is expressed as follows:[12]

$$-\boldsymbol{\nabla}\cdot\boldsymbol{q} = \rho c_v\frac{\partial T}{\partial t} + T_a\beta\frac{\partial \varepsilon_{ii}}{\partial t}, \tag{6}$$

where ρ and c_v are the mass density and specific heat per unit mass of the material, respectively. Parameter $\beta = E\alpha/(1-2\nu)$ is the thermal modulus. Variable ε_{ii} is also called volumetric strain, which is equal to the trace of strain tensor $\boldsymbol{\varepsilon}$. Now, by combining Eqs. (5) and (6) and eliminating $\boldsymbol{q}$, one can achieve the constitutive relation of heat conduction corresponding to GK model as follows:

$$k\nabla^2 T = \left(1 + \tau\frac{\partial}{\partial t} - 3l^2\nabla^2\right)\left(\rho c_v \frac{\partial T}{\partial t} + T_a\beta\frac{\partial \varepsilon_{ii}}{\partial t}\right). \tag{7}$$

By employing Eqs. (1), (3) and (4), the following relation for volumetric strain is derived:

$$\varepsilon_{ii} = -(1-2\nu)\frac{x}{R_0^2}\left(w + \frac{\partial^2 w}{\partial\theta^2}\right) + 2(1+\nu)\alpha T. \tag{8}$$

By inserting Eq. (8) into Eq. (7) and simplifying the obtained equation, one can attain the following equation:

$$\begin{aligned}\chi\nabla^2 T - \left[1 + \frac{2(1+\nu)}{1-2\nu}\Delta_E\right]\left(1 + \tau\frac{\partial}{\partial t} - 3l^2\nabla^2\right)\frac{\partial T}{\partial t} \\ = -\frac{\Delta_E}{\alpha}\left(1 + \tau\frac{\partial}{\partial t} - 3l^2\nabla^2\right)\frac{\partial}{\partial t}\left[\frac{x}{R_0^2}\left(w + \frac{\partial^2 w}{\partial\theta^2}\right)\right],\end{aligned} \tag{9}$$

where $\chi = k/\rho c_v$ and $\Delta_E = E\alpha^2 T_a/\rho c_v$. The value of parameter Δ_E is usually small, that is $\Delta_E \ll 1$. Therefore, Eq. (9) takes the following form:

$$\begin{aligned}\chi\nabla^2 T - \left(1 + \tau\frac{\partial}{\partial t} - 3l^2\nabla^2\right)\frac{\partial T}{\partial t} \\ = -\frac{\Delta_E}{\alpha}\left(1 + \tau\frac{\partial}{\partial t} - 3l^2\nabla^2\right)\frac{\partial}{\partial t}\left[\frac{x}{R_0^2}\left(w + \frac{\partial^2 w}{\partial\theta^2}\right)\right].\end{aligned} \tag{10}$$

3. Derivation of Temperature Distribution

By considering simple harmonic oscillations, one can express temperature change T and radial displacement w as follows:[24]

$$T = T_0(R,\theta,z)e^{i\omega_n t}, \tag{11}$$

$$w = W_n \sin(n\theta)e^{i\omega_n t}. \tag{12}$$

Here, parameter ω_n represents the nth frequency of oscillation determined as follows:[24]

$$\omega_n = \frac{n\left(n^2-1\right)}{\sqrt{n^2+1}}\sqrt{\frac{EI}{\rho A R_0^4}} \quad \text{for } n \geq 2, \tag{13}$$

where $I = \pi r_0^4/4$ and $A = \pi r_0^2$ introduce the moment of inertia and cross-sectional area, respectively. It can be written according to Fig. 1:

$$x = r\sin\phi, \tag{14}$$

$$z = r\cos\phi. \tag{15}$$

Substitution Eqs. (11), (12) and (14) into Eq. (10) results in

$$\begin{aligned}&\left(\chi + 3i\omega_n l^2\right)\nabla^2 T_0 - \left(i\omega_n - \tau\omega_n^2\right)T_0 \\ &\quad = -\frac{\Delta_E}{\alpha}\left(i\omega_n - \tau\omega_n^2 - 3i\omega_n l^2\nabla^2\right)\left[\frac{r\sin\phi}{R_0^2}(1-n^2)W_n\sin(n\theta)\right]\end{aligned} \tag{16}$$

The Laplacian operator is expressed as follows:[25]

$$\nabla^2 = \frac{\partial^2}{\partial R^2} + \frac{1}{R}\frac{\partial}{\partial R} + \frac{1}{R^2}\frac{\partial^2}{\partial\theta^2} + \frac{\partial^2}{\partial z^2}. \tag{17}$$

In thin rings, one can write $R_0 \gg x$. By considering this fact as well as Eq. (15) and relation $R = R_0 + x$, the Laplacian operator becomes:[25]

$$\nabla^2 = \frac{\partial^2}{\partial r^2} + \frac{1}{r}\frac{\partial}{\partial r} + \frac{1}{R_0^2}\frac{\partial^2}{\partial\theta^2} + \frac{1}{r^2}\frac{\partial^2}{\partial\phi^2}. \tag{18}$$

By inserting above relation into Eq. (16), applying operator ∇^2 to the right side of Eq. (16) and sorting the result, one can arrive at the following equation:

$$\begin{aligned}&\left(\chi + 3i\omega_n l^2\right)\left(\frac{\partial^2 T_0}{\partial r^2} + \frac{1}{r}\frac{\partial T_0}{\partial r} + \frac{1}{R_0^2}\frac{\partial^2 T_0}{\partial\theta^2} + \frac{1}{r^2}\frac{\partial^2 T_0}{\partial\phi^2}\right) - \left(i\omega_n - \tau\omega_n^2\right)T_0 \\ &\quad = -\frac{\Delta_E}{\alpha}\left(i\omega_n - \tau\omega_n^2 + 3i\omega_n l^2\frac{n^2}{R_0^2}\right)\left[\frac{r\sin\phi}{R_0^2}\left(1-n^2\right)W_n\sin\left(n\theta\right)\right].\end{aligned} \tag{19}$$

By looking carefully at the above partial differential equation, one can realize that this equation is Bessel type in terms of r and trigonometric type in terms of θ and ϕ. Therefore, similar to the approach used in the paper of Zhou *et al.*,[31] the trial function for T_0 based on the Galerkin approach can be expressed as follows:

$$T_0 = \sum_{p=1}^{\infty}\sum_{q=1}^{\infty} A_{pq} J_1\left(\frac{a_q}{r_0}r\right)\sin\left(p\theta\right)\sin\phi, \tag{20}$$

in which J_1 denotes the first-order Bessel function of first kind. It is assumed that the surface of ring is insulated, i.e. $\partial T_0/\partial r = 0$ at $r = r_0$. Substitution of Eq. (20) into this thermal boundary condition and utilization of the properties of Bessel functions yields

$$J_0(a_q) - J_2(a_q) = 0. \tag{21}$$

The details of deriving the above equation are given in the appendix. Table 1 contains the roots of a_q extracted by the numerical solution of the above equation. The

Table 1. The values of a_q.

q	1	2	3	4	5	6	7	8	9	10
a_q	1.841	5.331	8.536	11.706	14.864	18.016	21.164	24.311	27.457	30.602

orthogonality property of Bessel and trigonometric functions is employed for deriving the coefficients A_{pq}. How to use these properties has been completely explained in the paper of Li *et al.*[24] By inserting Eq. (20) into (15), multiplying the obtained equation by $rJ_1(\frac{a_j}{r_0}r)\sin(n\theta)\sin\phi$, and integrating the result over the entire volume of the ring, one can obtain:

$$A_{jn} = \frac{\Delta_E}{\alpha}\frac{2r_0}{R_0^2}\frac{(1-n^2)W_n}{(a_j^2-1)J_1(a_j)}\frac{(i\omega_n - \tau\omega_n^2)\tau_j}{(1+3i\omega_n\frac{l^2}{\chi})(1+\gamma_{jn}^2)+(i\omega_n-\tau\omega_n^2)\tau_j}, \tag{22}$$

where

$$\gamma_{jn} = \frac{n}{a_j}\frac{r_0}{R_0}. \tag{23}$$

$$\tau_j = \frac{r_0^2}{\chi a_j^2}. \tag{24}$$

By substituting Eq. (22) into Eq. (20), one can separate the real and imaginary parts of T_0 (i.e. $\mathrm{Re}(T_0)$ and $\mathrm{Im}(T_0)$) as follows:

$$\mathrm{Re}(T_0) = \frac{\Delta_E}{\alpha}\frac{2r_0}{R_0^2}(1-n^2)W_n\sin(n\theta)\sin\phi \sum_{j=1}^{\infty}\frac{J_1(\frac{a_j}{r_0}r)}{(a_j^2-1)J_1(a_j)}\frac{-\tau_j\tau\omega_n^2(1+\gamma_{jn}^2-\tau_j\tau\omega_n^2)+\tau_j\omega_n^2[3(1+\gamma_{jn}^2)\frac{l^2}{\chi}+\tau_j]}{(1+\gamma_{jn}^2-\tau_j\tau\omega_n^2)^2+[3(1+\gamma_{jn}^2)\frac{l^2}{\chi}+\tau_j]^2\omega_n^2}. \tag{25}$$

$$\mathrm{Im}(T_0) = \frac{\Delta_E}{\alpha}\frac{2r_0}{R_0^2}(1-n^2)W_n\sin(n\theta)\sin\phi \sum_{j=1}^{\infty}\frac{J_1(\frac{a_j}{r_0}r)}{(a_j^2-1)J_1(a_j)}\frac{\tau_j\omega_n(1+\gamma_{jn}^2-\tau_j\tau\omega_n^2)+\tau_j\tau\omega_n^3[3(1+\gamma_{jn}^2)\frac{l^2}{\chi}+\tau_j]}{(1+\gamma_{jn}^2-\tau_j\tau\omega_n^2)^2+[3(1+\gamma_{jn}^2)\frac{l^2}{\chi}+\tau_j]^2\omega_n^2}. \tag{26}$$

4. Determination of TED Value

Based on the definition of TED in thermal energy approach, the amount of TED is estimated via the following relation:[15]

$$Q^{-1} = \frac{1}{2\pi}\frac{\Delta U}{U_{\max}}, \tag{27}$$

in which Q refers to the quality factor of the vibrating resonator. Moreover, ΔU represents the dissipated thermal energy per cycle of oscillation, and $U_{\max}$ denotes the most strain energy in the resonator during a cycle of vibration. The dissipated thermal energy in an oscillating resonator during a cycle of vibration can be calculated by:[92]

$$\Delta U = -\pi \iiint_V \hat{\sigma}_{ij} \mathrm{Im}\left(\hat{\varepsilon}_{ij}^{th}\right) dV, \tag{28}$$

where V denotes the volume of the vibrating body. Additionally, the symbol $\wedge$ is a sign for the maximum magnitude of a variable during a cycle of oscillation. According to Eq. (28), the value of ΔU in a toroidal ring is given by

$$\Delta U = -\pi \iiint_V \hat{\sigma}_{\theta\theta} \mathrm{Im}\left(\alpha T_0\right) dV. \tag{29}$$

By using Eqs. (1), (3) and (11), and ignoring thermal stress, the following relations can be obtained:

$$\hat{\varepsilon}_{\theta\theta} = -\frac{x}{R_0^2}(1-n^2)W_n \sin(n\theta) = -\frac{r\sin\phi}{R_0^2}(1-n^2)W_n \sin(n\theta). \tag{30}$$

$$\hat{\sigma}_{\theta\theta} = -\frac{Ex}{R_0^2}(1-n^2)W_n \sin(n\theta) = -\frac{Er\sin\phi}{R_0^2}(1-n^2)W_n \sin(n\theta). \tag{31}$$

Furthermore, the following relation is true for a circular cross-sectional ring:

$$dV = (R_0 + x)d\theta \cdot rd\phi \cdot dr = (R_0 + r\sin\phi)d\theta \cdot rd\phi \cdot dr. \tag{32}$$

Substitution of Eqs. (26), (31) and (32) into Eq. (28) and integration over the entire volume of the ring yields the following result for ΔU:

$$\Delta U = \Delta_E \cdot \pi^2 EIR_0 \left[\frac{(1-n^2)W_n}{R_0^2}\right]^2 \times \sum_{j=1}^{\infty} \frac{8}{a_j^2(a_j^2-1)} \frac{\tau_j\omega_n(1+\gamma_{jn}^2-\tau_j\tau\omega_n^2)+\tau_j\tau\omega_n^3[3(1+\gamma_{jn}^2)\frac{l^2}{\chi}+\tau_j]}{(1+\gamma_{jn}^2-\tau_j\tau\omega_n^2)^2+[3(1+\gamma_{jn}^2)\frac{l^2}{\chi}+\tau_j]^2\omega_n^2}. \tag{33}$$

The amount of $U_{\max}$ is also calculated as follows:[92]

$$U_{\max} = \frac{1}{2}\iiint_V \hat{\sigma}_{ij}\hat{\varepsilon}_{ij} dV. \tag{34}$$

The above relation takes the following form for a ring:

$$U_{\max} = \frac{1}{2}\iiint_V \hat{\sigma}_{\theta\theta}\hat{\varepsilon}_{\theta\theta} dV. \tag{35}$$

Utilization of Eqs. (30)–(32) into Eq. (35) leads to:

$$U_{\max} = \frac{\pi EIR_0}{2}\left[\frac{(1-n^2)W_n}{R_0^2}\right]^2. \tag{36}$$

By substituting Eqs. (33) and (36) into Eq. (27), one can achieve the following expression for TED in circular cross-sectional miniaturized rings corresponding to 3D-GK model:

$$Q_{3D}^{-1} = \Delta_E \sum_{j=1}^{\infty} C_j \frac{\tau_j \omega_n (1 + \gamma_{jn}^2 - \tau_j \tau \omega_n^2) + \tau_j \tau \omega_n^3 [3(1 + \gamma_{jn}^2)\frac{l^2}{\chi} + \tau_j]}{(1 + \gamma_{jn}^2 - \tau_j \tau \omega_n^2)^2 + [3(1 + \gamma_{jn}^2)\frac{l^2}{\chi} + \tau_j]^2 \omega_n^2}, \tag{37}$$

where C_j is called the weighting coefficient, which is obtained from the following relation:

$$C_j = \frac{8}{a_j^2(a_j^2 - 1)}. \tag{38}$$

5. Results and Discussion

5.1. *Convergence study*

In this subsection, a convergence study is +performed to determine the sufficient number of terms appearing in Eq. (37) to reach a convergent and reliable response. As the first step, the values of the weighting coefficients C_j are calculated by using the roots of Eq. (21). For the first 10 terms, the results of these calculations are given in Table 2. As it is evident, when the value of j ascends, the value of the weighting coefficient C_j lessens significantly. Although the weighting coefficient C_j is a part of solution, and not all of it, it can be clearly seen that with the increase of the value of j, its impact on the result disappears swiftly. In the next step, the ratio of TED value by considering 1, 2 and ... up to 10 terms of the presented solution to TED value obtained by including 10 terms of this solution is depicted in Fig. 2 for 2D and 3D models. Indeed, in this figure, Q_j^{-1} and Q_{10}^{-1} represent the value of TED including the first j terms and the first 10 terms of the proposed solution, respectively. To extract these curves, a ring made of silicon (Si) with geometric parameters $r_0 = 500\,\text{nm}$ and $r_0/R_0 = 0.05$ at ambient temperature $T_a = 293\,K$ is considered. The mechanical and thermal properties of Si at some ambient temperatures are given in Table 3. The nonlocal parameter l is assumed to be 40 nm. As can be seen, for all considered vibrational modes, with the increase of

Table 2. The values of weighting coefficients C_j.

j	1	2	3	4	5
C_j	0.987	0.010	$1.528 * 10^{-3}$	$4.292 * 10^{-4}$	$1.647 * 10^{-4}$
C_1/C_j	1	98.7	645.942	2299.627	5992.714
j	6	7	8	9	10
C_j	$7.618 * 10^{-5}$	$3.996 * 10^{-5}$	$2.294 * 10^{-5}$	$1.409 * 10^{-5}$	$9.132 * 10^{-6}$
C_1/C_j	12956.156	24699.700	43025.283	70049.681	108081.472

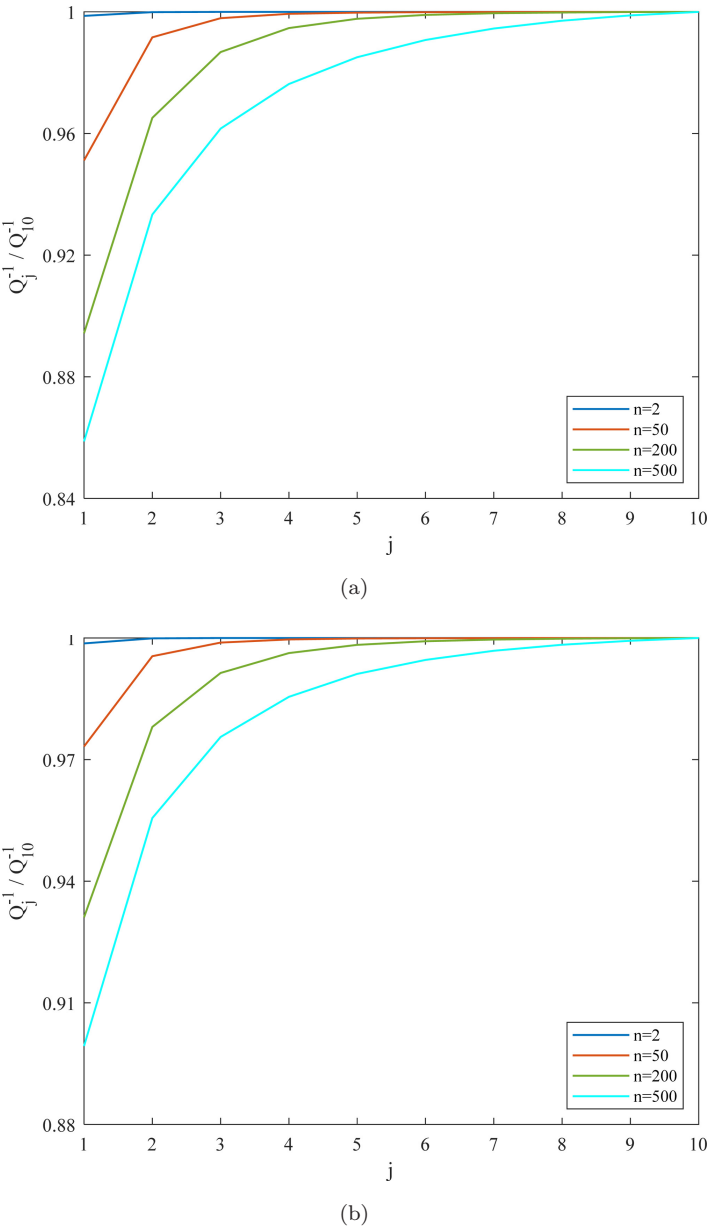

Fig. 2. Convergence study for a ring with $r_0 = 500\,\text{nm}$ and $r_0/R_0 = 0.05$ for (a) 2D (b) 3D models.

Table 3. Mechanical and thermal constants of silicon at different ambient temperatures.[21]

T_a (K)	E (GPa)	ρ (kg/m^3)	k (WmK)	ρc_v (J/m^{3}K)	α ($10^{-6}/K$)	τ (ps)
40	169.3	2330	3660	0.1^*10^6	−0.164	1511.13
80	169.2	2330	1360	0.4^*10^6	−0.472	140.46
160	168.5	2330	375	1.1^*10^6	0.689	14.14
293	165.9	2330	156	1.7^*10^6	2.59	3.87
400	163.1	2327	105	1.8^*10^6	3.253	2.5

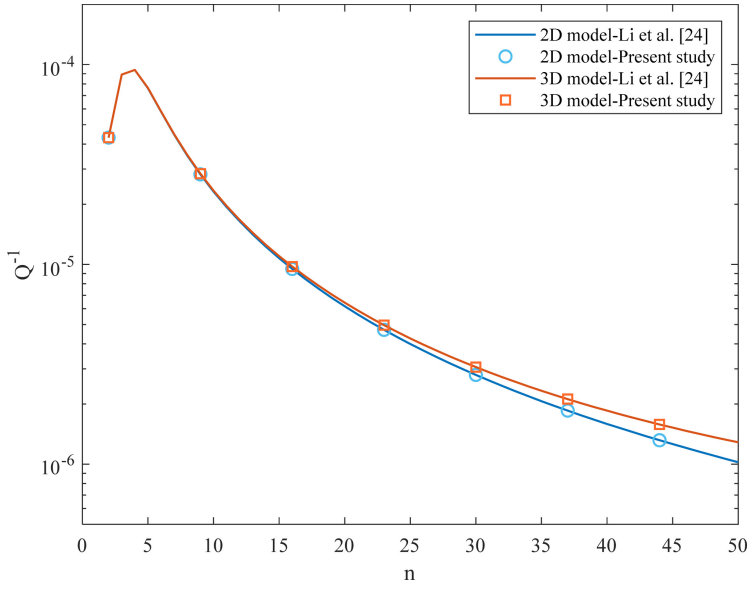

Fig. 3. Comparison of the results of this study with the results in the literature.

the terms involved in the calculations, the value of TED rapidly converges to the result obtained by accounting for the first 10 terms. Hence, it can be concluded that taking into account the first 10 terms of the solution given in Eq. (37) is enough to attain an answer with high accuracy.

5.2. *Validation of developed model*

This subsection is devoted to examination of the validity and accuracy of the presented formulation. For this purpose, the outcomes of this paper are compared with the results of the research of Li *et al.*,[24] in which an analytical model for TED in circular cross-sectional microrings has been established according to classical heat conduction or the Fourier model. In other words, to compare the findings of this work and those of Li *et al.*,[24] the phase lag parameter τ and nonlocal parameter

l should be set to zero. It should also be mentioned that to calculate TED in 2D model, it is enough to set parameter γ_{jn} in Eq. (37) equal to zero. In Fig. 3, the variations of TED with respect to mode number n is displayed for a ring with $r_0 = 10\,\mu$m and $r_0/R_0 = 0.02$. The properties of the ring material at temperature $T_a = 300\,$K are $E = 157\,$GPa, $\rho = 2330\,\text{kgm}^{-3}$, $c_v = 699.6\,\text{Jkg}^{-1}\text{K}^{-1}$, $\alpha = 2.6 * 10^{-6}\,\text{K}^{-1}$, $k = 90\,\text{Wm}^{-1}\text{K}^{-1}$. It is also to be noted that the first 10 terms of the presented solution are used to derive the results. As it is clear, the curves extracted via the presented relation and those reported by Li *et al.*[24] match each other. This agreement can be a proof of the accuracy and validity of the model provided in this study.

6. Numerical Examples

Through a detailed parametric study, this subsection surveys the dependence of TED value on some determining factors. The simulation results are derived for rings made of Si by making use of the first 10 terms of the presented solution. According to what has been mentioned in Refs. 93 and 94, by means of a quantitative approach, the value of relaxation time can be estimated in terms of measurable macroscopic parameters through the relation $\tau = 3\chi\rho/E$. Mechanical and thermal properties of Si at different ambient temperatures, including phase lag parameter τ, are listed in Table 3.[21] As for the nonlocal parameter l, which can be defined by the mean free path of energy carriers, different values have been reported for some materials. For instance, nonlocal parameter of silicon has been determined about 20-100 nm.[47,95] The average amount of nonlocal parameter of graphene at room temperature has been estimated to be 100 nm.[96] In another study, via molecular dynamics (MD) simulation, nonlocal parameter of graphene has been reported as 80 nm.[97] Moreover, for copper (Cu) and gold (Au), the ranges of 36-40 nm and 31-40 nm have been reported for nonlocal parameter.[31] Accordingly, in the present work, l has been chosen in the interval of –80 nm to examine the impact of size on heat conduction domain. Except for the cases where the influence of ambient temperature on the amount of TED is discussed, the rest of numerical results are given for ambient temperature $T_a = 293\,$K.

In Figs. 4(a) and 4(b), the effect of nonlocal parameter l on the variations of TED with respect to vibration mode number n is illustrated for $r_0/R_0 = 0.05$ and $r_0/R_0 = 0.01$, respectively. The results are provided for a ring with $r_0 = 20\,$nm. The curves indicate that in lower vibration modes, GK model predicts a lower value for TED than the Fourier model. Besides, by increasing the amount of nonlocal parameter l, a smaller value of TED is obtained. The rationale behind this finding is that the Fourier model assumes that thermal signals propagate through diffusion process in materials, while GK model by considering the phase lag parameter τ anticipates a wave-like propagation with finite velocity for thermal signals. Due to finite velocity of heat transfer, generated thermal signals do not have adequate

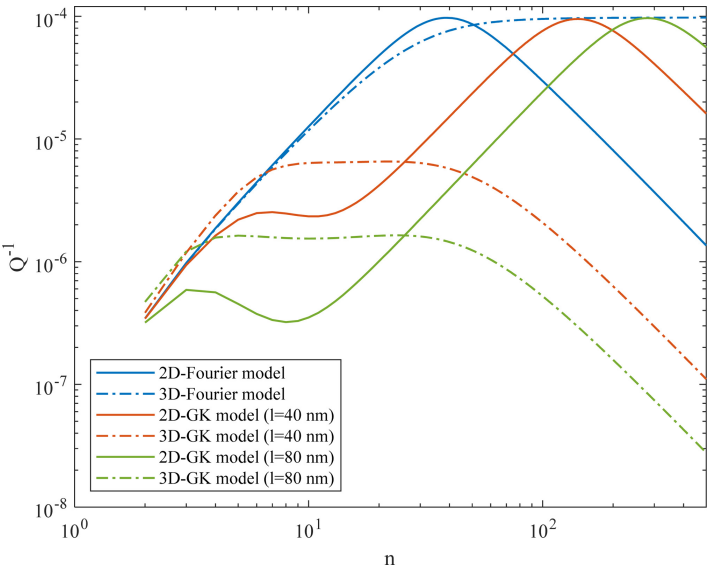

(a)

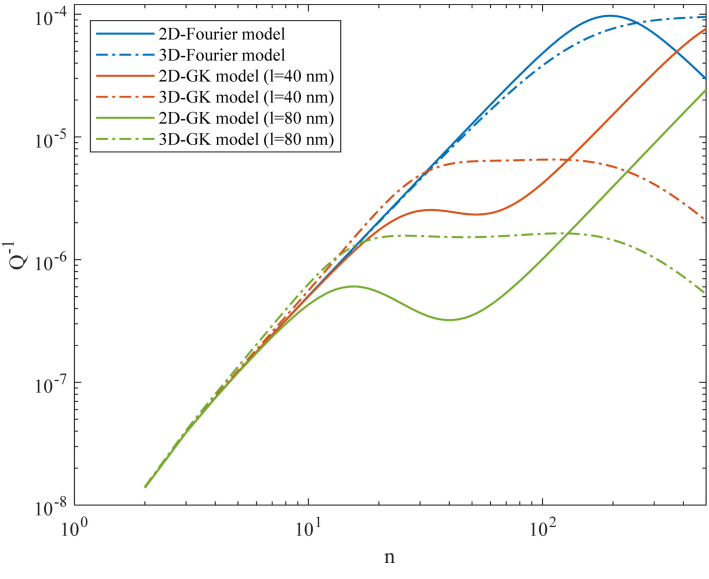

(b)

Fig. 4. The effect of nonlocal parameter l on the variations of TED in a ring with $r_0 = 20\,\text{nm}$ for (a) $r_0/R_0 = 0.05$ (b) $r_0/R_0 = 0.01$.

time for transition during the vibration, which weakens energy loss caused by TED. Additionally, given the inclusion of nonlocal effect in GK model, the temperature of an arbitrary point in a thermoelastic medium is affected by its adjacent points. This causes more energy to be brought by energy carriers from neighboring points. Given all these issues, GK model predicts lower TED values compared to the Fourier model. The effects of the Fourier and GK models on 2D and 3D cases of heat transfer are opposite, so that in low frequency modes, for the classical model, the estimation of 2D case is higher than the 3D case. This prediction for GK model is completely contrary in such a way that in low vibrational mode numbers, the approximation of 2D case is smaller than the 3D case.

Figures 5(a) and 5(b) are similar to Figs. 4(a) and 4(b), but for case $r_0 = 1\,\mu$m. As it is clear, because the size of the ring is considered larger in these diagrams, the impact of the nonlocal parameter lessens so that in a larger range of vibration mode numbers, the difference between the outcomes of the Fourier and GK models is small. It is also apparent that similar to case $r_0 = 20\,$nm, in low frequency modes, the use of GK model leads to smaller amounts for TED. Also, the comparison of Figs. 4 and 5 reveals that with the increase in the size of the ring, the peak value of TED occurs in much lower frequency mode numbers. As mentioned earlier, to derive the results of 2D model, it is enough to set term γ_{jn} equal to zero in Eq. (37). From this, it can be concluded that the discrepancy between 2D and 3D models is minimized when parameter γ_{jn} has a negligible value. According to the relation $\gamma_{jn} = (n/a_j)(r_0/R_0)$, this case occurs when either the mode number n is a small value or the magnitude of the ratio r_0/R_0 is slight (in other words, the ring is thin). This issue is clearly evident in Figs. 4 and 5. But for cases where the amount of γ_{jn} is considerable and cannot be ignored, due to the presence of γ_{jn} in both the numerator and denominator of Eq. (37), TED will be an intricate function in terms of γ_{jn}, which makes it convoluted to derive a specific pattern for TED for 2D and 3D situations of heat conduction.

For vibration modes $n = 2$ and $n = 20$, TED versus the geometrical ratio R_0/r_0 is depicted in Figs. 6(a) and 6(b), respectively. These plots are presented for the case $r_0 = 20\,$nm. According to these figures, in low frequency modes n or high ratios of R_0/r_0, the difference between the evaluation of 2D and 3D models diminishes. Figures 7(a) and 7(b) are drawn with the same conditions as Figs. 6(a) and 6(b), with the only difference that $r_0 = 1\,\mu$m is assumed. As can be seen, given the assumption that the ring is larger in Fig. 7, the difference between the results of the Fourier and GK models is reduced compared to Fig. 6, which is due to the decline in size effect.

Figures 8(a) and 8(b) examine the influence of ambient temperature T_a on the variations of TED with respect to the geometrical ratio R_0/r_0 for 2D-Fourier model and 2D-GK model ($l = 80\,$nm), respectively. To achieve these results, $r_0 = 200\,$nm and $n = 10$ are considered. From these curves, one can deduce that for both the

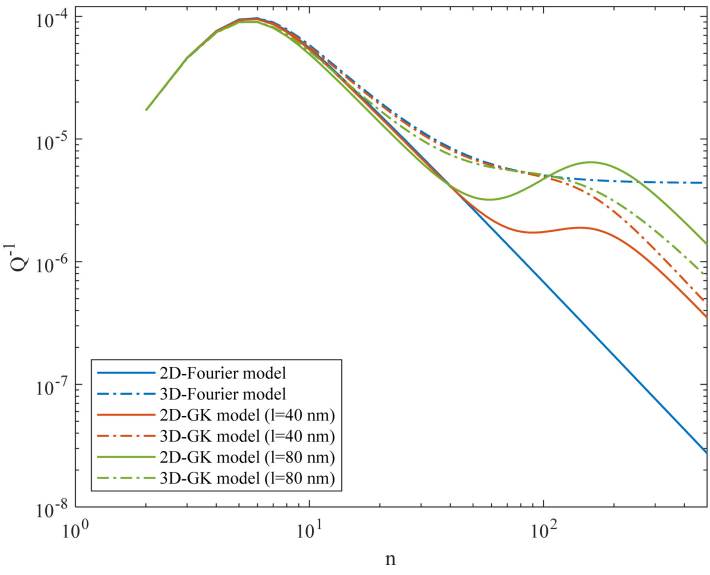

(a)

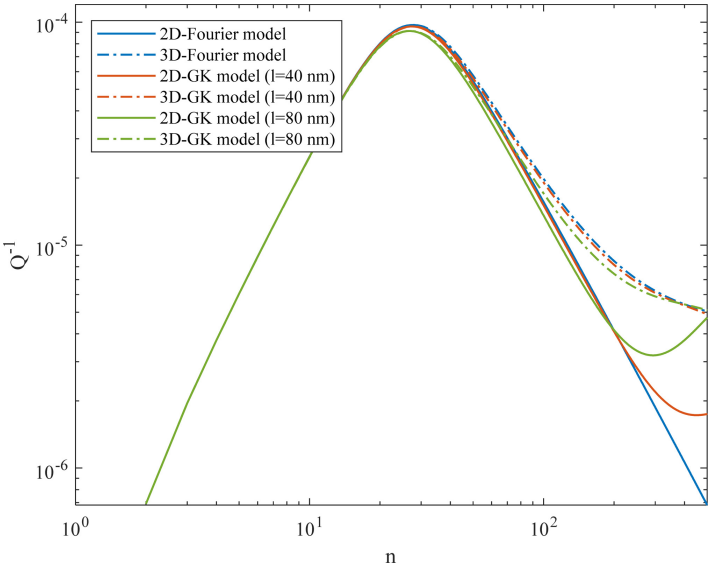

(b)

Fig. 5. The effect of nonlocal parameter l on the variations of TED in a ring with $r_0 = 1\,\mu$m for (a) $r_0/R_0 = 0.05$ (b) $r_0/R_0 = 0.01$.

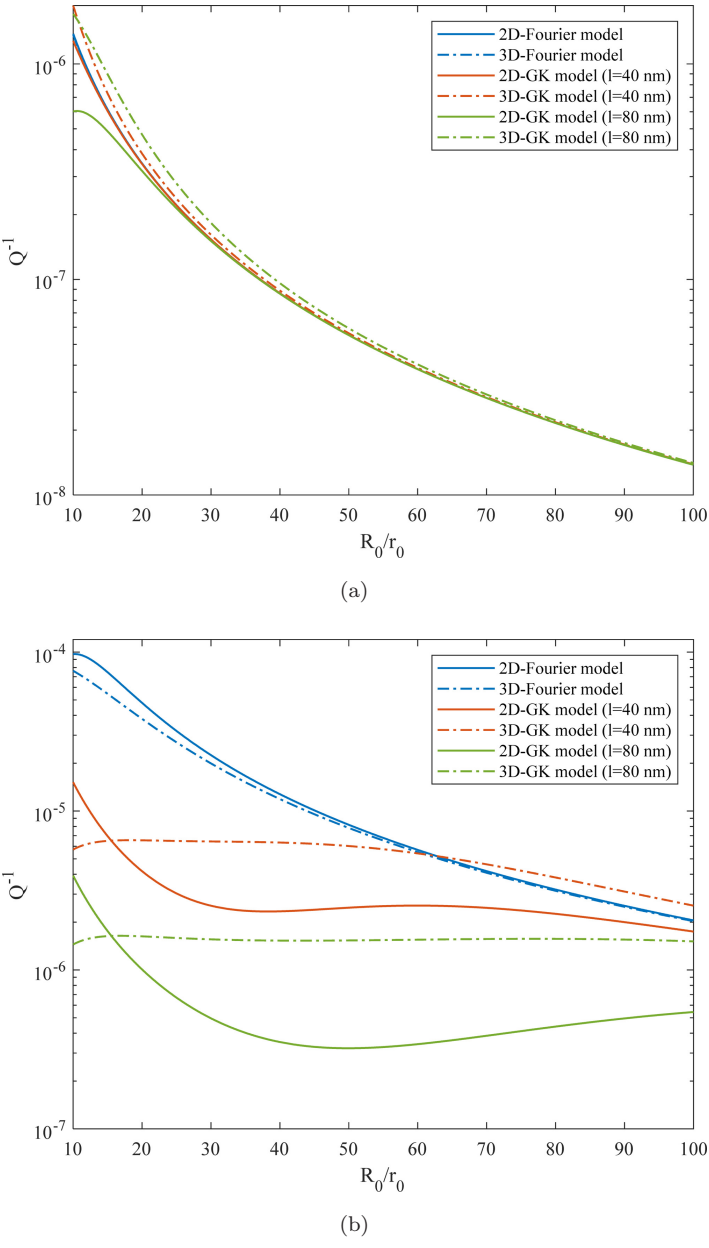

Fig. 6. TED versus the geometrical ratio R_0/r_0 for a ring with $r_0 = 20\,\text{nm}$ for (a) $n = 2$ (b) $n = 20$.

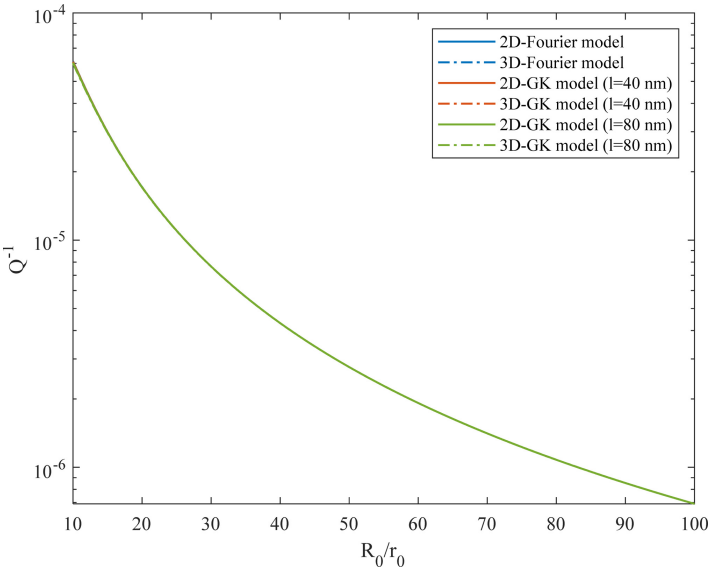

(a)

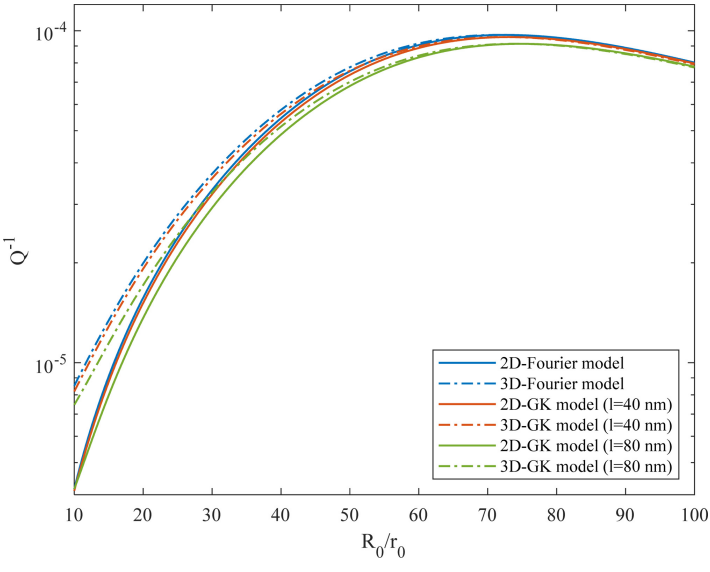

(b)

Fig. 7. TED versus the geometrical ratio R_0/r_0 for a ring with $r_0 = 1\,\mu$m for (a) $n = 2$ (b) $n = 20$.

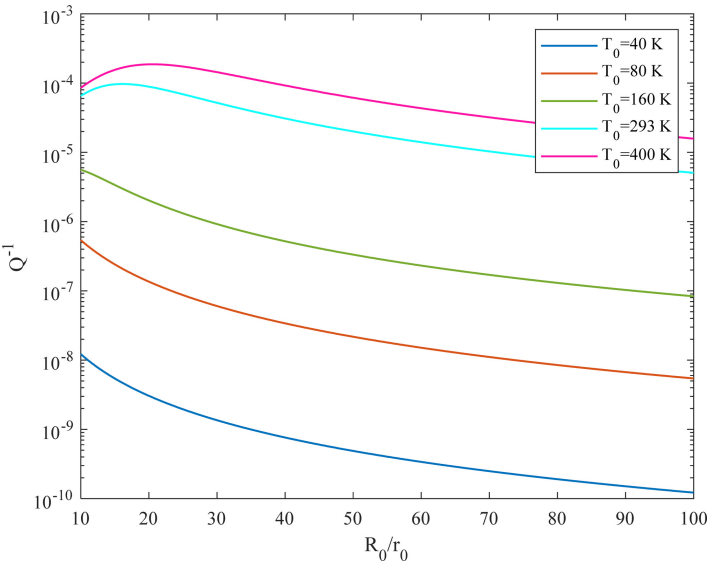

(a)

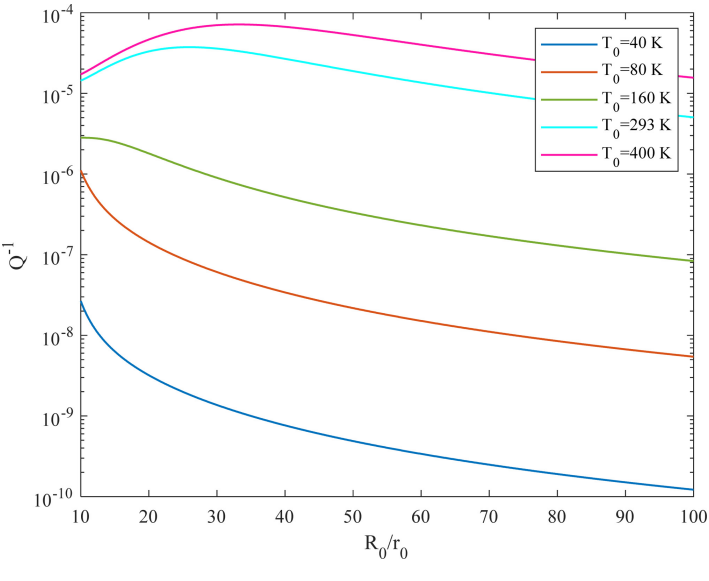

(b)

Fig. 8. The influence of ambient temperature T_a on the variations of TED with respect to the geometrical ratio R_0/r_0 with $r_0 = 200\,\text{nm}$ and $n = 10$ for (a) 2D-Fourier model (b) 2D-GK model ($l = 80\,\text{nm}$).

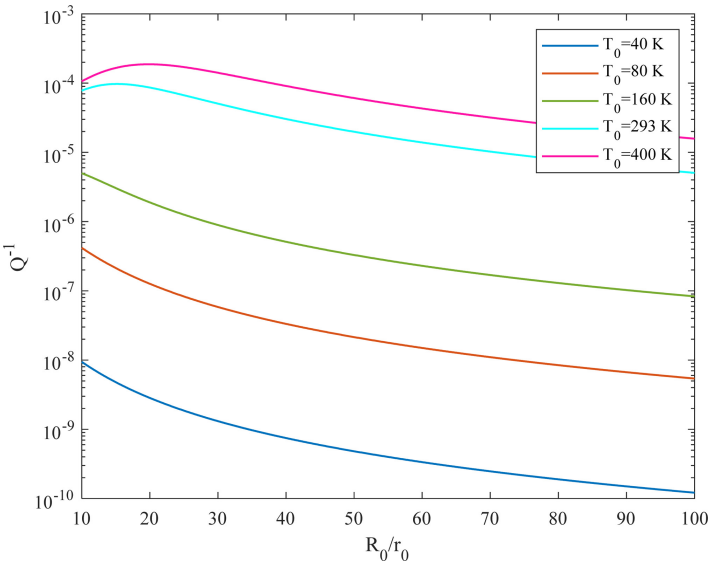

(a)

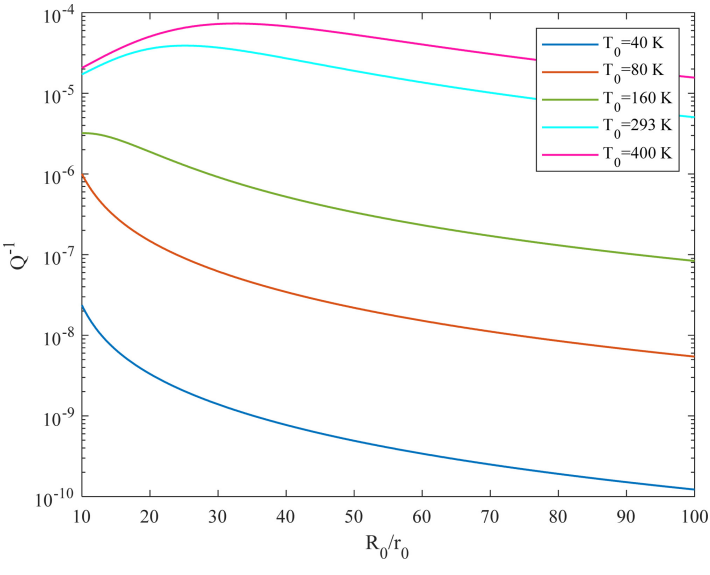

(b)

Fig. 9. The influence of ambient temperature T_a on the variations of TED with respect to the geometrical ratio R_0/r_0 with $r_0 = 200\,\text{nm}$ and $n = 10$ for (a) 3D-Fourier model (b) 3D-GK model ($l = 80\,\text{nm}$).

Fourier and GK models, TED is strengthened by the rise in the ambient temperature. It can also be observed that the impact of GK model on the magnitude of TED depends on the ambient temperature, so that at higher (lower) temperatures, the value of TED anticipated on the basis of GK model is less (more) than that computed by the Fourier model. These curves confirm that TED is a principal source of energy dissipation at room temperature. Figures 9(a) and 9(b) are drawn with the same conditions as Figs. 8(a) and 8(b), except that the curves are plotted based on 3D heat conduction model. It is evident that the results of the Fourier and GK models are remarkably different at low ratios of R_0/r_0, but with the increase of ratio R_0/r_0, which means that the size of the ring becomes larger, the effect of size weakens and the difference between the results of the Fourier and GK models is reduced.

7. Concluding Remarks

In the present work, with the help of Guyer–Krumhansl (GK) heat conduction model, a non-Fourier formulation for TED in small-sized rings with circular cross-section has been developed. To achieve this goal, the size-dependent equation of heat conduction in a circular cross-sectional ring has been firstly extracted in the scope of GK model. By solving this equation, the temperature field in the ring has been derived. In the next stage, by inserting the temperature distribution in definition of TED in thermal energy approach, an analytical relation consisting of phase lag and nonlocal parameters has been presented for estimation of TED value. The section of numerical results has been divided into three subsections. In the first subsection, a convergence study has been performed to determine the number of terms required to reach the exact answer. In the second subsection, the precision of established formulation has been checked by way of a comparison study. In the third subsection, the sensitivity of the amount of TED to some crucial factors like scale parameters of GK model, geometric features of ring, number of vibration modes and ambient temperature has been appraised through graphical presentation. The main findings of this study can be listed as follows:

- The influence of GK model on the variation of TED is deeply sensitive to ambient temperature and mode number, so that in small order modes, for low (high) ambient temperatures, the estimation of GK model for TED is more (less) than that of the Fourier model.
- GK model predicts more peak points than the Fourier model for the curves of TED variations with vibration mode.
- By enlargement of r_0 (for fixed ratio R_0/r_0) or by enlargement of the ratio R_0/r_0 (for fixed value of r_0), the impact of size and GK model on the amount of TED fades gradually.

- The discrepancy between the estimations of 2D and 3D models is less for lower vibration mode numbers and thinner rings.
- By ascending the ambient temperature, TED intensifies.

Appendix

According to the properties of Bessel functions of the first kind, one can write:

$$\frac{dJ_n(\lambda r)}{dr} = \lambda J_{n-1}(\lambda r) - \frac{n}{r} J_n(\lambda r). \tag{A1}$$

$$J_{n-2}(\lambda r) = \frac{2(n-1)}{\lambda r} J_{n-1}(\lambda r) - J_n(r). \tag{A2}$$

By inserting $n = 1$ into Eq. (A1), one can get:

$$\frac{dJ_1(\lambda r)}{dr} = \lambda J_0(\lambda r) - \frac{1}{r} J_1(\lambda r). \tag{A3}$$

Moreover, by placing $n = 2$ into Eq. (A2), the following relation is obtained:

$$J_0(\lambda r) = \frac{2}{\lambda r} J_1(\lambda r) - J_2(\lambda r). \tag{A4}$$

Sorting the above relation gives:

$$J_1(\lambda r) = \frac{\lambda r}{2} [J_0(\lambda r) + J_2(\lambda r)]. \tag{A5}$$

Substitution of Eq. (A5) into Eq. (A3) yields the following relation:

$$\frac{dJ_1(\lambda r)}{dr} = \frac{\lambda}{2} \left[J_0 \left(\lambda r \right) - J_2 \left(\lambda r \right) \right]. \tag{A6}$$

By considering Eq. (20), setting $\lambda = a_q/r_0$ and applying thermal boundary condition $\partial T_0/\partial r = 0$ at $r = r_0$, the use of above relation leads to:

$$\frac{a_q}{2r_0} [J_0(a_q) - J_2(a_q)] = 0. \tag{A7}$$

The nontrivial solutions of above equation are determined via the following equation:

$$J_0(a_q) - J_2(a_q) = 0. \tag{A8}$$

References

1. F. Ayazi and K. Najafi, A HARPSS polysilicon vibrating ring gyroscope, *J. Microelectromech. Syst.* **10**(2) (2001) 169–179.
2. A. K. Rourke, S. McWilliam and C. H. J. Fox, Frequency trimming of a vibrating ring-based multi-axis rate sensor, *J. Sound Vib.* **280**(3–5) (2005) 495–530.
3. R. Eley, C. H. J. Fox and S. McWilliam, The dynamics of a vibrating-ring multi-axis rate gyroscope, *Proc. Inst. Mech. Eng. C J. Mech. Eng. Sci.* **214**(12) (2000) 1503–1513.

4. M. H. Li, C. Y. Chen, C. S. Li, C. H. Chin and S. S. Li, Design and characterization of a dual-mode CMOS-MEMS resonator for TCF manipulation, *J. Microelectromech. Syst.* **24**(2) (2014) 446–457.
5. B. Walter, M. Faucher, E. Algré, B. Legrand, R. Boisgard, J. P. Aimé and L. Buchaillot, Design and operation of a silicon ring resonator for force sensing applications above 1 MHz, *J. Micromech. Microeng.* **19**(11) (2009) 115009.
6. Y. Ding, X. Zhu, S. Xiao, H. Hu, L. H. Frandsen, N. A. Mortensen and K. Yvind, Effective electro-optical modulation with high extinction ratio by a graphene–silicon microring resonator, *Nano Lett.* **15**(7) (2015) 4393–4400.
7. W. Zhou, J. He, L. Ran, L. Chen, L. Zhan, Q. Chen and B. Peng, A piezoelectric microultrasonic motor with high Q and good mode match, *IEEE/ASME Trans. Mechatronics* **26**(4) (2021) 1773–1781.
8. F. Zangeneh-Nejad and R. Safian, A graphene-based THz ring resonator for label-free sensing, *IEEE Sens. J.* **16**(11) (2016) 4338–4344.
9. M. Chester, Second sound in solids, *Phys. Rev.* **131**(5) (1963) 2013.
10. R. A. Guyer and J. A. Krumhansl, Dispersion relation for second sound in solids, *Phys. Rev.* **133**(5A) (1964) A1411.
11. H. W. Lord and Y. Shulman, A generalized dynamical theory of thermoelasticity, *J. Mech. Phys. Solids* **15**(5) (1967) 299–309.
12. D. Y. Tzou, *Macro-to Microscale Heat Transfer: The Lagging Behavior* (John Wiley & Sons, 2014).
13. R. A. Guyer and J. A. Krumhansl, Solution of the linearized phonon Boltzmann equation, *Phys. Rev.* **148**(2) (1966) 766.
14. A. E. Green and P. Naghdi, Thermoelasticity without energy dissipation, *J. Elasticity* **31**(3) (1993) 189–208.
15. C. Zener, Internal friction in solids. I. Theory of internal friction in reeds, *Phys. Rev.* **52**(3) (1937) 230.
16. R. Lifshitz and M. L. Roukes, Thermoelastic damping in micro-and nanomechanical systems, *Phys. Rev. B* **61**(8) (2000) 5600.
17. S. J. Wong, C. H. J. Fox and S. McWilliam, Thermoelastic damping of the in-plane vibration of thin silicon rings, *J. Sound Vib.* **293**(1-2) (2006) 266–285.
18. P. Lu, H. P. Lee, C. Lu and H. B. Chen, Thermoelastic damping in cylindrical shells with application to tubular oscillator structures, *Int. J. Mech. Sci.* **50**(3) (2008) 501–512.
19. P. Li, Y. Fang and R. Hu, Thermoelastic damping in rectangular and circular microplate resonators, *J. Sound Vib.* **331**(3) (2012) 721–733.
20. Y. Fang and P. Li, Thermoelastic damping in thin microrings with two-dimensional heat conduction, *Physica E Low-dimensional Syst. Nanostruct.* **69** (2015) 198–206.
21. H. Zhou, P. Li and Y. Fang, Single-phase-lag thermoelastic damping models for rectangular cross-sectional micro-and nano-ring resonators, *Int. J. Mech. Sci.* **163** (2019) 105132.
22. H. Zhou and P. Li, Dual-phase-lagging thermoelastic damping and frequency shift of micro/nano-ring resonators with rectangular cross-section, *Thin-Walled Struct.* **159** (2021) 107309.
23. C. Xiao, G. Zhang, P. Hu, Y. Yu, Y. Mo and V. Borjalilou, Size-dependent generalized thermoelasticity model for thermoelastic damping in circular nanoplates, *Waves Random Complex Media* (2021) 1–21, DOI: 10.1080/17455030.2021.1968538.
24. P. Li, Y. Fang and J. Zhang, Thermoelastic damping in microrings with circular cross-section, *J. Sound Vib.* **361** (2016) 341–354

25. J. H. Kim and J. H. Kim, Thermoelastic attenuation of circular-cross-sectional micro/nanoring including single-phase-lag time, *Int. J. Mech. Mater. Des.* **17**(4) (2021) 915–929.
26. F. Li and S. Esmaeili, On thermoelastic damping in axisymmetric vibrations of circular nanoplates: incorporation of size effect into structural and thermal areas, *Eur. Phys. J. Plus* **136**(2) (2021) 1–17.
27. Y. Tai and N. Chen, Thermoelastic damping in the out-of-plane vibration of a microring resonator with rectangular cross-section, *Int. J. Mech. Sci.* **151** (2019) 684–691.
28. I. A. Abbas and A. D. Hobiny, Analytical solution of thermoelastic damping in a nanoscale beam using the fractional order theory of thermoelasticity, *Int. J. Struct. Stab. Dyn.* **16**(9) (2016) 1550064.
29. H. Zhou, P. Li, H. Jiang, H. Xue and B. Bo, Nonlocal dual-phase-lag thermoelastic dissipation of size-dependent micro/nano-ring resonators, *Int. J. Mech. Sci.* **219** (2022) 107080.
30. H. Kumar and S. Mukhopadhyay, Thermoelastic damping analysis for size-dependent microplate resonators utilizing the modified couple stress theory and the three-phase-lag heat conduction model, *Int. J. Heat Mass Transf.* **148** (2020) 118997.
31. H. Zhou, D. Shao, X. Song and P. Li, Three-dimensional thermoelastic damping models for rectangular micro/nanoplate resonators with nonlocal-single-phase-lagging effect of heat conduction, *Int. J. Heat Mass Transf.* **196** (2022) 123271.
32. H. Zhou and P. Li, Nonlocal dual-phase-lagging thermoelastic damping in rectangular and circular micro/nanoplate resonators, *Appl.ied Math. Modelling* **95** (2021) 667–687.
33. V. Borjalilou and M. Asghari, Size-dependent analysis of thermoelastic damping in electrically actuated microbeams, *Mech. Adv. Mater. Struct.* **28**(9) (2021) 952–962.
34. H. Zhou, D. Shao and P. Li, Thermoelastic damping and frequency shift in micro/nano-ring resonators considering the nonlocal single-phase-lag effect in the thermal field, *Appl. Math. Modelling* **115** (2023) 237–258.
35. H. Farokhi and M. H. Ghayesh, Nonlinear thermo-mechanical behaviour of MEMS resonators, *Microsyst. Technol.* **23**(12) (2017) 5303–5315.
36. A. M. Zenkour, A. E. Abouelregal and I. A. Abbas, Generalized thermoelastic vibration of an axially moving clamped microbeam subjected to ramp-type thermal loading, *J. Therm. Stresses* **37**(11) (2014) 1302–1323.
37. D. Liu, T. Geng, H. Wang and S. Esmaeili, Analytical solution for thermoelastic oscillations of nonlocal strain gradient nanobeams with dual-phase-lag heat conduction, *Mech. Based Des. Struct. Mach.* (2021) 1–31, DOI: 10.1080/15397734.2021.1987261.
38. H. Zhou and P. Li, Thermoelastic damping in micro-and nanobeam resonators with non-Fourier heat conduction, *IEEE Sens. J.* **17**(21) (2017) 6966–6977.
39. G. Prateek, D. Sarthak, R. Vasudevan, M. Haboussi and M. Ganapathi, Large amplitude free vibration analysis of isotropic curved nano/microbeams using a nonlocal sinusoidal shear deformation theory-based finite element method, *Int. J. Struct. Stab. Dyn.* **21**(5) (2021) 2150074.
40. W. Weng, Y. Lu and V. Borjalilou, Size-dependent thermoelastic vibrations of Timoshenko nanobeams by taking into account dual-phase-lagging effect, *Eur. Phys. J. Plus* **136**(7) (2021) 1–26.
41. H. Zhang, L. Li, W. Ma, Y. Luo, Z. Li and H. Kuai, Effects of welding residual stresses on fatigue reliability assessment of a PC beam bridge with corrugated steel webs under dynamic vehicle loading, in *Structures*, Vol. 45 (Elsevier, 2022), pp. 1561–1572.

42. M. Gu, X. Cai, Q. Fu, H. Li, X. Wang and B. Mao, Numerical analysis of passive piles under surcharge load in extensively deep soft soil, *Buildings* **12**(11) (2022) 1988.
43. A. Ebrahimi-Mamaghani, R. Sotudeh-Gharebagh, R. Zarghami and N. Mostoufi, Thermo-mechanical stability of axially graded Rayleigh pipes, *Mech. Based Des. Struct. Mach.* **50**(2) (2022) 412–441.
44. S. Akkoca, S. M. Bagdatli and N. Kara Togun, Nonlinear vibration movements of the mid-supported micro-beam, *Int. J. Struct. Stab. Dyn.* https://doi.org/10.1142/S0219455422501747.
45. V. Borjalilou, M. Asghari and E. Bagheri, Small-scale thermoelastic damping in microbeams utilizing the modified couple stress theory and the dual-phase-lag heat conduction model, *J. Therm. Stresses* **42**(7) (2019) 801–814.
46. C. Luo, L. Wang, Y. Xie and B. Chen, A new conjugate gradient method for moving force identification of vehicle–bridge system, *J. Vib. Eng. Technol.* (2022) 1–18, https://doi.org/10.1007/s42417-022-00824-1.
47. H. Zhang, T. Kim, G. Choi and H. H. Cho, Thermoelastic damping in micro-and nanomechanical beam resonators considering size effects, *Int. J. Heat Mass Transf.* **103** (2016) 783–790.
48. A. Ebrahimi-Mamaghani, A. Forooghi, H. Sarparast, A. Alibeigloo and M. I. Friswell, Vibration of viscoelastic axially graded beams with simultaneous axial and spinning motions under an axial load, *Appl. Math. Modelling* **90** (2021) 131–150.
49. H. Sarparast, A. Alibeigloo, V. Borjalilou and O. Koochakianfard, Forced and free vibrational analysis of viscoelastic nanotubes conveying fluid subjected to moving load in hygro-thermo-magnetic environments with surface effects, *Arch. Civil Mech. Eng.* **22**(4) (2022) 1–28.
50. X. Yue, X. Yue and V. Borjalilou, Generalized thermoelasticity model of nonlocal strain gradient Timoshenko nanobeams, *Arch. Civil Mech. Eng.* **21**(3) (2021) 1–20.
51. A. Ebrahimi-Mamaghani, R. Sotudeh-Gharebagh, R. Zarghami and N. Mostoufi, Dynamics of two-phase flow in vertical pipes, *J. Fluids Struct.* **87** (2019) 150–173.
52. H. Zhou, H. Jiang, P. Li, H. Xue and B. Bo, Thermoelastic damping in the size-dependent micro/nanobeam resonator with nonlocal dual-phase-lag heat conduction, *Thin-Walled Struct.* **169** (2021) 108437.
53. A. T. Jalil, Z. M. Saleh, A. F. Imran, Y. Yasin, A. A. K. Ruhaima, A. Gatea and S. Esmaeili, A size-dependent generalized thermoelasticity theory for thermoelastic damping in vibrations of nanobeam resonators, *Int. J. Struct. Stab. Dynamics*, https://doi.org/10.1142/S021945542350133X.
54. J. N. Yu, C. She, Y. P. Xu and S. Esmaeili, On size-dependent generalized thermoelasticity of nanobeams, *Waves Random Complex Media* (2022) 1–30.
55. F. Shayestenia and M. Ghadiri, Investigation of flexoelectric effect on nonlinear vibration and dynamic instability of piezoelectric sandwich micro/nanobeam using the nonlocal strain gradient theory, *Int. J. Struct. Stab. Dyn.* **23**(4) (2022) 2350045.
56. H. Zhou, P. Li and Y. Fang, Thermoelastic damping in circular cross-section micro/nanobeam resonators with single-phase-lag time, *Int. J. Mech. Sci.* **142** (2018) 583–594.
57. H. Zhang, Z. Ouyang, L. Li, W. Ma, Y. Liu, F. Chen and X. Xiao, Numerical study on welding residual stress distribution of corrugated steel webs, *Metals* **12**(11) (2022) 1831.
58. A. E. Mamaghani, S. E. Khadem and S. Bab, Vibration control of a pipe conveying fluid under external periodic excitation using a nonlinear energy sink, *Nonlinear Dyn.* **86**(3) (2016) 1761–1795.

59. I. A. Abbas, Exact solution of thermoelastic damping and frequency shifts in a nanobeam resonator, *Int. J. Struct. Stab. Dyn.* **15**(6) (2015) 1450082.
60. V. Borjalilou, M. Asghari and E. Taati, Thermoelastic damping in nonlocal nanobeams considering dual-phase-lagging effect, *J. Vib. Control* **26**(11-12) (2020) 1042–1053.
61. H. Zhou, P. Li, W. Zuo and Y. Fang, Dual-phase-lag thermoelastic damping models for micro/nanobeam resonators, *Appl. Math. Modelling* **79** (2020) 31–51.
62. H. L. Dai, X. Yan and L. Yang, Thermoelastic transient behavior for a clamped FGM circular plate, *Int. J. Struct. Stab. Dyn.* **14**(4) (2014) 1450005.
63. F. S. Alzahrani and I. A. Abbas, Generalized photo-thermo-elastic interaction in a semiconductor plate with two relaxation times, *Thin-Walled Struct.* **129** (2018) 342–348.
64. B. Singh, H. Kumar and S. Mukhopadhyay, Analysis of size effects on thermoelastic damping in the Kirchhoff's plate resonator under Moore–Gibson–Thompson thermoelasticity, *Thin-Walled Struct.* **180** (2022) 109793.
65. Z. Li, Q. Zhang, H. Shen, X. Xiao, H. Kuai and J. Zheng, Buckling performance of the encased functionally graded porous composite liner with polyhedral shapes reinforced by graphene platelets under external pressure, *Thin-Walled Struct.* **183** (2023) 110370.
66. J. Chen, H. Tong, J. Yuan, Y. Fang and R. Gu, Permeability prediction model modified on kozeny-carman for building foundation of clay soil, *Buildings* **12**(11) (2022) 1798.
67. S. Liu, J. Ma, X. Yang, Y. Sun, J. Yang and X. Wang, Theoretical 3D model of thermoelastic damping in laminated rectangular plate resonators, *Int. J. Struct. Stab. Dyn.* **18**(12) (2018) 1850158.
68. V. Borjalilou and M. Asghari, Thermoelastic damping in strain gradient microplates according to a generalized theory of thermoelasticity. *J. Thermal Stresses*, **43**(4) (2020) 401–420.
69. J. Chu, Y. Wang, S. Sahmani and B. Safaei, (2022). Nonlinear large-amplitude oscillations of PFG composite rectangular microplates based upon the modified strain gradient elasticity theory, *Int. J. Struct. Stab. Dyn.* **22**(6) (2020) 2250068.
70. A. Ghobadi, H. Golestanian, Y. T. Beni and K. K. Żur (2021). On the size-dependent nonlinear thermo-electro-mechanical free vibration analysis of functionally graded flexoelectric nano-plate, *Commun. Nonlinear Sci. Numer. Simul.* **95** (2020) 105585.
71. V. Borjalilou and M. Asghari, Small-scale analysis of plates with thermoelastic damping based on the modified couple stress theory and the dual-phase-lag heat conduction model, *Acta Mech.* **229**(9) (2018) 3869–3884.
72. R. Gholami and R. Ansari, Thermal postbuckling of temperature-dependent functionally graded nanocomposite annular sector plates reinforced by carbon nanotubes, *Int. J. Struct. Stab. Dyn.* **21**(2) (2021) 2150026.
73. X. Ge, P. Li, Y. Fang and L. Yang, Thermoelastic damping in rectangular microplate/nanoplate resonators based on modified nonlocal strain gradient theory and nonlocal heat conductive law, *J. Therm. Stresses* **44**(6) (2021) 690–714.
74. C. Xiao, G. Zhang, P. Hu, Y. Yu, Y. Mo and V. Borjalilou, Size-dependent generalized thermoelasticity model for thermoelastic damping in circular nanoplates, *Waves Random Complex Media* (2021) 1–21, DOI: 10.1080/17455030.2021.1968538.
75. A. Ghobadi, Y. T. Beni and H. Golestanian, Nonlinear thermo-electromechanical vibration analysis of size-dependent functionally graded flexoelectric nano-plate exposed magnetic field, *Arch. Appl. Mech.* **90**(9) (2020) 2025–2070.
76. R. K. Bhangale and N. Ganesan, A linear thermoelastic buckling behavior of functionally graded hemispherical shell with a cut-out at apex in thermal environment, *Int. J. Struct. Stab. Dyn.* **5**(2) (2005) 185–215.

77. V. Borjalilou and M. Asghari, Mathematical modeling of anisotropic hyperelastic cylindrical thick shells by incorporating thickness deformation and compressibility with application to arterial walls, *Int. J. Struct. Stab. Dyn.* **22**(13) (2022) 2250141.
78. M. Li, Y. Cai, L. Bao, R. Fan, H. Zhang, H. Wang and V. Borjalilou, Analytical and parametric analysis of thermoelastic damping in circular cylindrical nanoshells by capturing small-scale effect on both structure and heat conduction, *Arch. Civil Mech. Eng.* **22**(1) (2022) 1–16.
79. J. Sun, S. Sahmani and B. Safaei, Nonlinear dynamical instability characteristics of FG piezoelectric microshells incorporating nonlocality and strain gradient size dependencies, *Int. J. Struct. Stab. Dyn.* (2022) 2350074, https://doi.org/10.1142/S0219455423500748.
80. W. B. Ning and D. Z. Wang, Dynamic and stability response of a cylindrical shell subjected to viscous annular flow and thermal load, *Int. J. Struct. Stab. Dyn.* **16**(10) (2016) 1550072.
81. M. Li, Y. Cai, R. Fan, H. Wang and V. Borjalilou, Generalized thermoelasticity model for thermoelastic damping in asymmetric vibrations of nonlocal tubular shells, *Thin-Walled Struct.* **174** (2022) 109142.
82. R. Alshenawy, S. Sahmani, B. Safaei, Y. Elmoghazy, A. Al-Alwan and M. Al Nuwairan, (2023). Three-dimensional nonlinear stability analysis of axial-thermal-electrical loaded FG piezoelectric microshells via MKM strain gradient formulations, *Appl. Math. Comput.* **439** (2022) 127623.
83. I. A. Abbas, Eigenvalue approach on fractional order theory of thermoelastic diffusion problem for an infinite elastic medium with a spherical cavity, *Appl. Math. Modelling* **39**(20) (2015) 6196–6206.
84. Huang, Z., Li, T., Huang, K., Ke, H., Lin, M., & Wang, Q. Predictions of flow and temperature fields in a T-junction based on dynamic mode decomposition and deep learning, *Energy* **261** (2022) 125228.
85. I. A. Abbas, Analytical solution for a free vibration of a thermoelastic hollow sphere, *Mech. Based Des. Struct. Mach.* **43**(3) (2015) 265–276.
86. I. A. Abbas and A. M. Zenkour, Dual-phase-lag model on thermoelastic interactions in a semi-infinite medium subjected to a ramp-type heating, *J. Comput. Theor. Nanosci.* **11**(3) (2014) 642–645.
87. J. Yang, L. Y. Fu, Y. Zhang and T. Han, Temperature-and pressure-dependent pore microstructures using static and dynamic moduli and their correlation, *Rock Mech. Rock Eng.* **55** (2022) 1–20.
88. J. Zhang, C. Zhang and Q. Xue, Insight into energy dissipation behavior of a SDOF structure controlled by the pounding tuned mass damper system, *Earthq. Eng. Struct. Dyn.* **51**(4) (2022) 958–973.
89. I. A. Abbas, A GN model based upon two-temperature generalized thermoelastic theory in an unbounded medium with a spherical cavity, *Appl. Math. Comput.* **245** (2014) 108–115.
90. A. D. Hobiny and I. A. Abbas, Theoretical analysis of thermal damages in skin tissue induced by intense moving heat source, *Int. J. Heat Mass Transf.* **124** (2018) 1011–1014.
91. D. Xiao, Y. Hu, Y. Wang, H. Deng, J. Zhang, B. Tang and G. Li, Wellbore cooling and heat energy utilization method for deep shale gas horizontal well drilling, *Appl. Therm. Eng.* **213** (2022) 118684.
92. A. S. Nowick, *Anelastic Relaxation in Crystalline Solids*, Vol. 1 (Elsevier, 2012).

93. M. Chester, Second sound in solids, *Phys. Rev.* **131**(5) (1963) 2013
94. Z. F. Khisaeva and M. Ostoja-Starzewski, Thermoelastic damping in nanomechanical resonators with finite wave speeds, *J. Therm. Stresses* **29**(3) (2006) 201–216.
95. R. Maranganti and P. Sharma, Length scales at which classical elasticity breaks down for various materials, *Phys. Rev. Lett.* **98**(19) (2007) 195504.
96. M. H. Bae, Z. Li, Z. Aksamija, P. N. Martin, F. Xiong, Z. Y. Ong and E. Pop, Ballistic to diffusive crossover of heat flow in graphene ribbons, *Nat. Commun.* **4**(1) (2013) 1–7.
97. X. Xu, L. F. Pereira, Y. Wang, J. Wu, K. Zhang, X. Zhao and B. Özyilmaz, Length-dependent thermal conductivity in suspended single-layer graphene, *Nat. Commun.* **5**(1) (2014) 1–6.